A Highly Compensated Interferometer for Biochemical Analysis

Michael N. Kammer[1,2], Amanda K. Kussrow[1], Ian R. Olmsted[1] and Darryl J. Bornhop*[1]

[1]Vanderbilt Department of Chemistry and Vanderbilt Institute of Chemical Biology

[2]Vanderbilt Department of Biomedical Engineering

ABSTRACT: Here we report an improved interferometric sensing approach that facilitates high sensitivity nanovolume refractive index (RI) measurements and molecular interaction assays without a temperature controller. The compensated backscattering interferometer (CBSI) is based on a Helium-Neon (He-Ne) laser, microfluidic chip, and a CCD array. CBSI enables simultaneous differential RI measurements within nanoliter volumes, at a compensation level of ca. 5×10^{-8} RIU in the presence of large thermal perturbations (8°C). This level of dn/dT compensation is enabled by elongating the laser beam along the central axis of the microfluidic channel and measuring the difference in positional shift of interference patterns from two adjacent regions of the channel. By separating two solutions by an air gap or oil droplet, CBSI can discriminate the difference in RI for the sample and reference at a detection limit of 7×10^{-7} RIU in the absence of electronic filtering. At this level of ΔRI sensitivity, it is possible to perform label-free, free-solution biochemical assays at the 10's of nM level without the typical high-resolution temperature control needed in conventional interferometers. Here we illustrate the effective use of CBSI by quantifying the binding affinities for mannose - Concanavalin A and Ca^{2+} - Recoverin interactions.

Keywords: Compensated Interferometry, Microfluidics, Temperature insensitivity, Free-solution Assay, Label-Free determinations

Interaction assays have led to significant scientific discoveries in the biochemical, medical and chemical disciplines. The basis of these inter- and intramolecular interactions include London dispersion, hydrogen bonding, hydrophobic character, and electrostatics. In the past three decades, the sophistication and power of techniques to interrogate these processes has developed at an unprecedented rate. These methods range from Nuclear Magnetic Resonance (NMR),[1] and Mass Spectrometry (MS)[2,3], to calorimetric[4,5] and thermophoretic.[6] Among the most commonly used label-free interaction assay methods are the refractive index (RI) methods[7], including Biolayer Interferometry (BLI)[8] and Surface Plasmon Resonance (SPR).[9] All of these methods have advantages, but the free-solution methods calorimetery and NMR are limited by sensitivity. Many other label-free methods, including BLI and SPR, require analyte immobilization onto the sensor surface, increasing assay complexity[10] and impacting performance when working within complex matrices. Backscattering interferometry (BSI) offers an alternative to these methods, providing free-solution operation,[11] complex matrix compatibility,[12] no sensitivity to the relative mass of the participating species,[13] and picogram/mL sensitivity.[14]

Numerous other interferometric methods have been used to perform biosensing determinations. These include the Mach–Zehnder interferometer (MZI), the Young interferometer (YI), the Hartman interferometer (HI), and the dual polarization interferometer. For a more detailed discussion of these interferometric methods we direct the reader to two reviews on interferometry in biosensing.[7,15] Not covered in these reviews are two methods, one is a variation of the porous Si surface sensing method[16] and the other is a hybrid approach using active and passive plasmonic interferometry.[17]

The first method has been reported to measure bovine serum albumin (BSA) adsorption in the range from 150 pM to 15 μM[18] and the use of electrical double layer (EDL)-induced accumulation of charged ions onto a negatively charged nanostructured surface of SiO_2 to give bulk measurements of ca. 10^{-7} RIU.[19] Here, a signal processing strategy based on subtracting before and after reflectance spectra provides an improvement over previous Si sensors. It is not clear just how the double layer system reported to provide bulk RI measurements might be used to perform solution-phase interaction studies. The second relatively new interferometric method uses fluorescence modulation of the interferometric signal allowing picoliter sample volumes to be interrogated.[20] This type of sensor can work with an incoherent source, providing detectable ΔRI changes estimated at $5x10^{-4}$ RIU in 1pL, but does require fluorescence modulation.[20] By comparison, BSI provides 10^{-6} - 10^{-7} RIU sensitivity in 350 pL volumes.[13]

One limitation of most interferometers is that they exhibit a significant level of temperature sensitivity.[21] However, it has been reported that the MZI can be configured in a manner to limit temperature-induced drift,[22] Also, because temperature variations affect the RI and physical thickness inversely, instrumental thermostatting is less stringent in the HI than in other interferometric methods.[23]

Here we report on a new interferometric design that addresses the thermal sensitivity problem, while allowing specific binding assays in free-solution, using the Free-SRF-BSI methodology.[13] FreeSRF capitalizes on background elimination by RI-matching the sample and reference,[24] yet up until now, these assays required the use of sequential measurements in the same channel of a microfluidic chip. The accuracy of such determinations can be impacted by temperature fluctuations and source instabilities that lead to changes in the measured RI. Thus, we have used a high-resolution temperature controller and a chip design to mitigate environmental perturbations of the laser beam in BSI.

The obvious solution to the sequential measurement approach is a sample-reference configuration. Two approaches to BSI we have investigated, two adjacent capillaries[25] and two channels in a chip.[26] In the first case, we effectively demonstrated sensitivity in the nanoRIU regime,[25] yet found the approach to be impractical due to alignment constraints and the necessity to encapsulate the capillaries. In the second case, we used a calcite beam splitter to produce two parallel, orthogonally polarized, equal intensity beams, which were used to illuminate two microfluidic channels etched into a micro-fluidic chip separated by 1mm.[26] This approach allowed binding assays to be performed, yet alignment was extremely tedious. Upon careful evaluation, we found the two-channel chip approach provided little environmental noise rejection, giving relatively low level of compensation. In theory, fabrication of microfluidic channels with channel diameter accuracy of ±5nm should allow for compensation, yet, aligning the two discrete, adjacent interferometers proved problematic requiring the use of a high-resolution temperature controller to compensate for room temperature variations. Now, we think it better to describe this optical train as a comparator, as opposed to a compensated interferometer.

Here we demonstrate an interferometric configuration with a high level of noise rejection, enabling operation in the *absence* of a temperature controller. The Compensated Backscattering Interferometer (CBSI), shown in Figure 1, uses a single elongated laser to interrogate adjacent regions of the same microfluidic channel simultaneously. The result in essentially two identical interferometers, providing compensation of temperature variations and source instabilities, such as wavelength and intensity wander. Relative RI determinations are performed by spatially separating two solutions (a binding sample and reference sample) with either air, oil, or hole in the chip) and then measuring the difference in spatial position of two discrete regions of an interference pattern (Figure 1). Here we demonstrate that CBSI provides a noise floor of ca. 10^{-8} RIU without environmental control and in the presence of an 8°C external temperature excursion. We also show mix-and-read FreeSRF binding assays with CBSI allowing the quantification of protein-ion (Ca^{2+} - Recoverin) and protein-small molecule (Concanavalin A (ConA) - mannose) interactions in nanoliter volumes, label-free and in free solution in the absence of a temperature controller.

EXPERIMENTAL SECTION

As shown in Figure 1, a helium-neon (He-Ne) laser (wavelength 632 nm, Melles Griot, USA) illuminates a channel in a microfluidic chip. The glass chip was obtained from Micronit Microtechnologies, (Netherlands), has an isotropically etched channel[27] that is nearly semi-circular with dimensions of (210 µm × 100 µm radius) and served as both the sample container and the resonator for the interferometer. The chip, side-view shown in Figure 1, has been described in detail elsewhere, with the modifications discussed below. Briefly, the He-Ne beam was shaped and conditioned by first passing it through a collimating lens (Oz Optics, Canada) giving a Gaussian beam diameter at $1/e^2$ of 0.8 mm. This beam was then stretched along one axis by a pair of anamorphic prism pairs, each with a 4-fold expansion (Thorlabs, New Jersey, USA). The prisms were arranged in series with identical orientation to produce a 16-fold expansion of the laser profile along one axis. The result was a beam that was about 12 mm in the long axis of the channel and ca. 0.8 mm width in short axis. Interrogation of the channel by the elongated laser results in a series of interference "fringes" as shown in Figure 1. The resulting fringe patterns were captured on a 2D CCD array (Basler, 12.8 mm × 9.625 mm, 5.5 μm^2 pixels) that is placed 10 cm from the channel in the nearly 0° backscatter direction. The black shadow in the center of the fringe pattern is produced by a 1mm hole drilled through the center of the channel allowing the sample and reference regions to be separated.

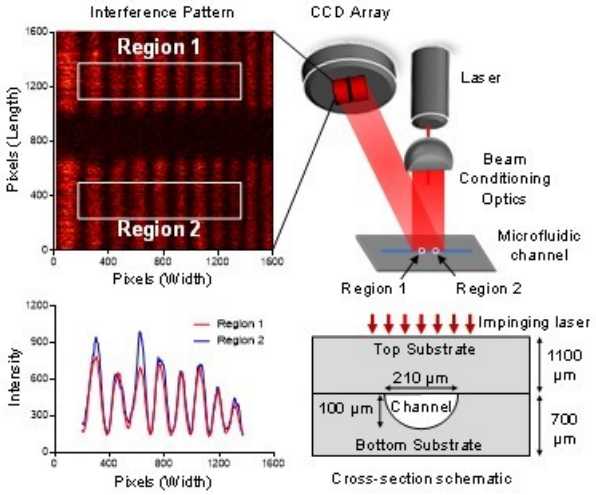

Figure 1. Block diagram of the Compensated Backscattering Interferometer. Chip schematic not drawn to scale.

Using an in-house Labview™ program, windows of the fringes from each detection zone measuring 200 pixels long × 1200 pixels wide were selected for further analysis. The fringe selection method was similar to the one previously reported for BSI,[28] consisting of choosing fringe windows with a nearly a single spatial frequency (Figure 1). The fringe positional shifts from each of these two windows were quantified by a fast Fourier transform (FFT), allowing for tracking of the phase of the dominant frequency over time.

The injection method used here takes advantage of the unique properties of microfluidic channels, capitalizing on the high surface tension of aqueous solutions and small dimensions of the channel.[29] The result is the ability to introduce samples unperturbed by a pressure source, using only capillary action to draw the droplets into chip. The hole drilled through the center microfluidic channel is large

enough to serve as a passive "fluid stop," preventing the sample/reference solutions from jumping across the gap. The added benefit of this injection approach is that the sample/reference solutions are introduced at constant pressure. The hole also serves as the waste collection site. For clarity, an injection is pictorially demonstrated in Figure 2 using red and green dye. As shown, 1 μL is pipetted into the chip inlet at either end of the channel (Figure 2C). Capillary action pulls the sample into the channel (Figure 2D), and then stops once the sample reaches the hole drilled in the center of the channel (Figure 2E).

Chip temperature was measured and controlled by a Peltier driven by a high-resolution temperature controller (Wavelength Electronics). Several precautions ensure optimum temperature regulation. The thermistor/thermal couple (Omega Engineering Inc., USA) and Peltier were selected of sufficient size and power and mounted in intimate contact with an Al block and cooling fins with a layer of thermal grease. We used only thermistor/thermal couples specified for use with the Wavelength Electronics integral-differential controller. The controller was recently calibrated and was positioned in the laboratory so as to be as far as possible from sources of temperature variations, such as those induced by heating and A/C cooling vents.

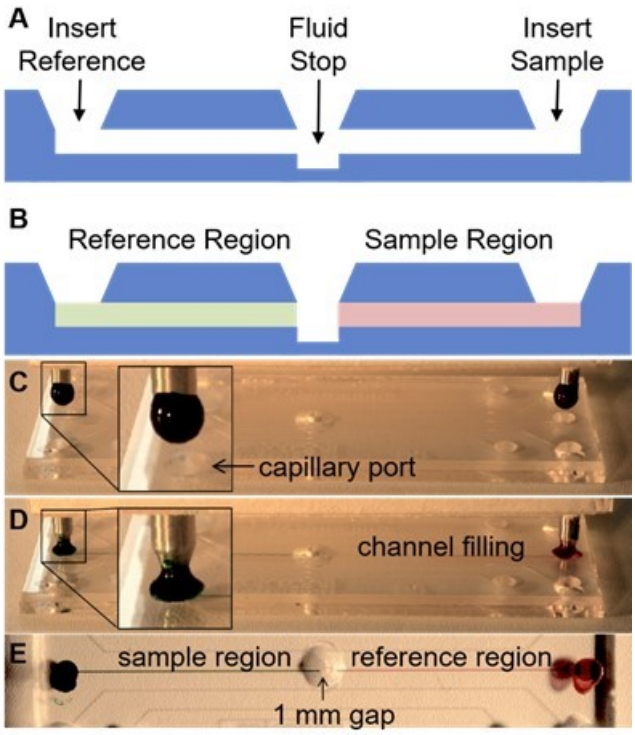

Figure 2. CBSI sample introduction scheme. A side-view schematic of the microfluidic chip showing (A) the hole through the channel to function as a fluid stop and (B) the channel filled with both reference and sample. (C-E) Pictoral demonstration of sample introduction.

Temperature compensation experiments were performed by injecting deionized (DI) water into both detection regions and measuring the phase difference between the two windows for five minutes to establish a baseline while the chip was held at a constant temperature of 25°C. Then, the temperature of the entire chip was increased (by the Peltier) in increments of 0.5°C and the phase shifts were recorded for one minute. Following the one-minute measurement, temperature was increased again by 0.5°C. This procedure was repeated until measurements had been made from 25-27°C. The experiment performed in triplicate. Glycerol 'compensation' determinations were performed by injecting the same concentration of glycerol (0, 0.5, 1, 3, and 5 mM in DI water) into both sides of the channel, and the phase shift were recorded for 30 seconds. Temperature was held constant at 25°C ± 0.001°C by the Peltier. After each measurement, the samples were removed by vacuum applied to the center hole, and the channel was rinsed with 100 μL of DI water and 100 μL Methanol. Concentrations were run from low to high and then the entire concentration range was repeated in triplicate. The glycerol 'calibration' experiment was performed using increasing concentrations of glycerol in Phosphate Buffered Saline (PBS) (0, 0.5, 1, 3, and 5 mM), introduced into the 'sample side' with PBS introduced into the 'reference side' of the chip. The measurement was performed by collecting 30 seconds of data for each sample-reference pair, in absence of temperature control. The channels were rinsed with 100 μL PBS, 100 μL methanol, and 100 μL deionized water and then dried for 2 minutes before injection of the next sample. This procedure was performed in triplicate.

CBSI stability in the presence of large ambient temperature changes was tested by placing the entire optical train in a temperature-controlled chamber, inducing large temperature changes, and measuring the baseline noise. First, we established the baseline of the un-thermostatted CBSI at ambient temperature (22°C) inside the enclosure. Then, we heated the box by 4°C and measured the baseline noise for 5 minutes. This experiment was repeated by heating the chamber by an additional 4°C allowing for compensation testing of an 8°C change in environment.

Binding assays were performed in an endpoint format.[13] Concanavalin A (ConA) and Mannose samples were prepared in a buffer containing 50mM Sodium Acetate, 1mM Ca^{2+}, and 1mM Mn^{2+} in deionized water. Binding samples consisted of increasing concentrations of Mannose (0-800 μM) incubated with 2μM ConA. Reference samples consisted of Mannose only. Samples were incubated at room temperature for 2 hours before measurement. Recoverin samples were prepared in modified Phosphate Buffered Saline (PBS) devoid of Ca^{2+} or Mg^{2+}. Binding samples consisted of increasing concentrations of Ca^{2+} (0-4 μM) in PBS incubated with 540 nM Recoverin (Novis Biologicals). Reference samples consisted of matched Ca^{2+} concentrations with no Recoverin present. Samples were incubated at room temperature for 1.5 hours with gentle agitation. Sample-reference differential measurements were recorded over 15 seconds for each replicate measurement. Total analysis time from the end of incubation to finalized data analysis is 1 hour. To obtain K_D, the data were fit to single-site saturation isotherms using Graphpad Prism (Graphpad Software, Inc.). Mannose, PBS, Ca^{2+}, and ConA were obtained from Sigma.

RESULTS AND DISCUSSION

Interferometer Design. We hypothesized that using an elongated beam to illuminate a chip, a high contrast fringe pattern (Figure 1) would allow for RI measurements in multiple locations along the channel simultaneously. Then, if

chip and beam non-uniformities could be effectively averaged and two samples could be separated by a gap or hole, the optical train would form nearly identical interferometers. In short, comparing solutions in the *same* channel with the *same laser* should result in a significant level of noise reduction.

To test this theory, we first evaluated CBSI by measuring the instrument response to large temperature changes imparted to the chip with deionized water in both sides of the channel. After recording the phase difference between the two windows for 5 minutes to establish a baseline, the temperature of the chip was increased in increments of 0.5°C from 25 - 27°C (Figure 3). The result of this temperature ramp experiment (ΔT = 2°C) was a linear response in phase change for both of the two sensing regions (R^2=0.9995), with the slopes equal to 146.3 ± 1.15 and 146.4 ± 1.18 mrad/°C respectively. The difference in these phase values provides a level of compensation of 0.57 mrad/°C, or a maximum baseline excursion of ΔRI of $1.8x10^{-6}$ over the entire range. Using the value of dn/dT for water of 1.06×10^{-4} RIU/°C (CRC Handbook of Chemistry and Physics) the total temperature induced perturbation corresponds to a ΔRI = $2.12x10^{-4}$. Here the differential measurement provided a 122-fold reduction in RI sensitivity to environmental noise.

Next, we tested noise compensation for samples consisting of solutions of glycerol in PBS, at increasing concentrations, but using the same concentration in both the sample and reference region. This approach allowed us to evaluate compensation in more complex PBS matrix. Here, each glycerol concentration exhibited the expected RIU change in each window for the analyte (11.38 ± 0.09 mrad/mM in region 1 and 11.41 ± 0.13 mrad/mM in region 2) with R^2=0.9994. In the absence of any electronic filtering, the difference or compensated signal exhibited a baseline response of 1.6×10^{-7} RIU/mM.

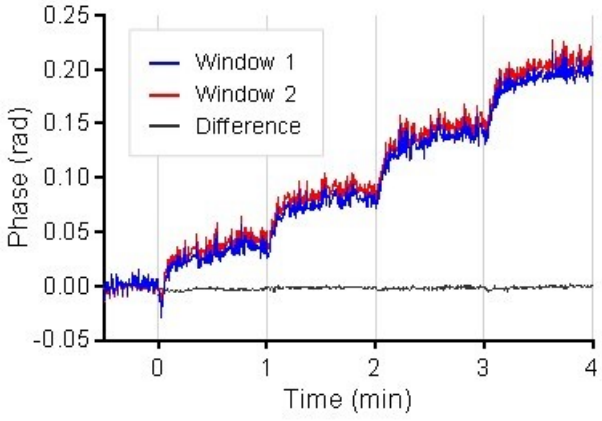

Figure 3. CBSI phase output as a function of time for a temperature ramp of 2°C in 0.5°C steps, in 1-minute intervals. The reference/sample windows are plotted in red and blue, with the compensated (difference) signal plotted in black.

Figure 4A presents results from an experiment where we compared the S/N performance of CBSI to BSI.[28] Here, the standard deviation of the baseline for BSI and CBSI is plotted with both systems thermally stabilized (red and blue bars in Figure 4A) and with CBSI operating *without temperature control* (green bar in Figure 4A). The first two plots result from measuring the magnitude of the noise/drift over 5 minutes (1.6 µRIU and 1.4 µRIU) for BSI and CBSI respectively. Surprisingly, when turning the Peltier off on the CBSI instrument, the equilibrium baseline noise further decreased from 1.4 µRIU to 1.04 µRIU. This is a 27% reduction in baseline noise over the "temperature-stabilized" configuration illustrating the noise floor for CBSI is lower in the absence of active temperature control. A possible explanation for this observation is that the integral differential controller driving the Peltier cannot operate at a resolution high enough to contain the noise floor below 1×10^{-6} RIU (ca. 0.009°C). As it cycles on and off based upon the measured temperature of the chip holder and the set point, minor temperature fluctuations will be induced by the Peltier causing the RI of the fluid to change.

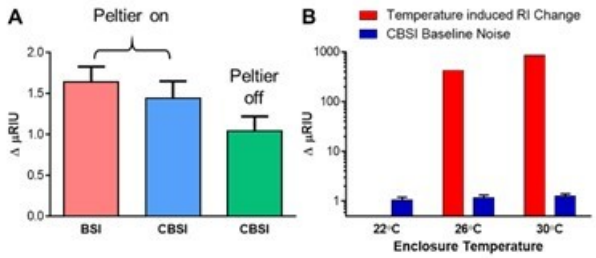

Figure 4. (A) BSI and CBSI baseline noise with and in the absence of thermal stabilization. Error bars represent standard deviation of 3 measurements. (B) CBSI baseline noise and predicted ΔRI from a 4°C and 8°C ambient temperature change to the entire optical train. Error bars represent standard deviation of 3 measurements.

In the real world, environmental perturbations are never confined to the microfluidic chip, but rather will affect the entire optical train. Therefore, we tested CBSI stability in the presence of large ambient temperature changes by placing the entire optical train in a temperature-controlled chamber and inducing large temperature changes. First, we established the baseline of the un-thermostated CBSI at ambient temperature (22°C) inside the enclosure (1.04 µRIU). Then we heated the box by 4°C and measured the baseline noise for 5 minutes. Using the dn/dT for water of 1.06×10^{-4} RIU/°C for a range of relevant temperatures (20-30°C), we calculated this 4°C change to correspond to a ΔRI of 424 µRIU (Figure 4B first red bar). CBSI exhibited very little sensitivity to this large thermal perturbation, reporting an increase in baseline noise of 1.2×10^{-7} RIU or 0.12 µRIU (error bar on second blue bar). Here the overall noise level of CBSI was 1.16 µRIU. Upon further raising the temperature of the enclosure another 4°C, (final temperature 30°C, second red bar, note Y axis is a log scale), we measured an increase in drift (noise over 5 minutes) of just 0.08 µRIU. Interestingly the total 8°C temperature change, corresponding to a substantial perturbation of 8.5×10^{-4} RIU (848µRIU) induced only a 2×10^{-7} RIU (0.20µRIU) increase in drift noise. In other words, CBSI compensates for a 4280-fold temperature-induced change in RIU without any electronic filtering. This level of compensation should enable use in environments with widely changing temperatures, including benchtop and remote locations.

Further testing CBSI *without* temperature control, we performed glycerol calibration curves in PBS. Here five glycerol concentrations (0, 0.5, 1, 3, and 5 mM) were analyzed in triplicate, producing a robust response with a slope

of 13.2 mRad/mM (1.25mRad/μRIU) and R^2 of 0.9996 (Figure 5). The LOD obtained without filtering or temperature control (measured as 3×baseline/slope) was found to be 7.0×10^{-7} RIU (0.11 mM glycerol) utilizing a baseline noise over 3 seconds of 0.39 μRIU. A more conservative value for performance, the LOQ (measured by 3×σ/slope) was calculated using the standard deviation of replicate injections (0.74 μRIU) and was found to be 1.8×10^{-6} RIU (1.8 μRIU or 0.17 mM glycerol). By applying a low pass filter (0.5 second time constant) to the data, the baseline noise was reduced to 2.8×10^{-8} RIU, resulting in an LOD of 6.7×10^{-8} RIU.

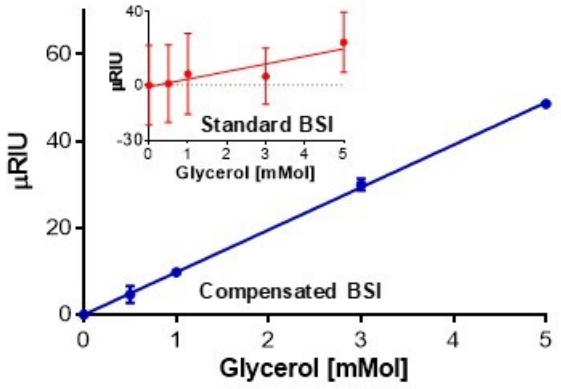

Figure 5. Calibration curve consisting of glycerol in PBS performed with no temperature control, on CBSI. Error bars represent standard deviation of 3 trials. Inset: The same experiment performed on a standard single channel BSI in the absence of temperature control.

For comparison, we performed the same calibration experiment on a single channel BSI instrument with *no temperature* control. Figure 5 inset illustrates the significant ambient temperature sensitivity of the interferometer, showing that over the course of each 10-minute calibration trial, the signal drifted by roughly -2.1×10^{-5} RIU. Furthermore, the reproducibility of replicate injections reported an LOQ of 14.14 mM glycerol (148 μRIU), over 80-fold poorer than for CBSI.

BSI has been shown to provide high quality binding affinities and even target quantitation at the level of several hundred molecules[12] when operating at level of ca. 10^{-6} RIU. Therefore, the LOQ provided by the CBSI of 1.8×10^{-6} RIU, in the absence of active thermal control, is well within performance criteria to allow free-solution molecular interaction assays. Here we chose two binding systems to illustrate the use of CBSI for measuring bimolecular interactions. The first system was Concanavalin A (ConA), a protein-small molecule interaction system, chosen because of its physiological importance and well documented properties.[30] The second binding system was the well-studied studied ion - protein interaction, Ca^{2+} binding the neuronal calcium sensor (NCS) recoverin.

The study of carbohydrate–lectin interactions spans a multitude of disciplines, from virology and neuroscience to glycomics and immunology. Purified lectins can be used in biorecognition,[31] such as blood typing, because various glycolipids and glycoproteins on an individual's red blood cells bind specifically to certain lectins. These principles of biorecognition can be applied to various diseases and have been used for *in-vitro* inhibition of HIV-1.[32] Because of the size mismatch in the binding partners (100,000 Da for ConA and 180 Da for the sugar) and the fact that carbohydrates do not usually contain functional groups that induce large changes in protein absorbance or fluorescence, quantitative determinations of binding affinities are often quite difficult to obtain. The installation of labels (fluorophores, spin labels, cross-linking agents) on the carbohydrate runs the risk of distorting the binding function that is being studied. Since CBSI is a label-free, free-solution measurement, we avoid these potential perturbations and/or limitation of labeled or tethered assays. Figure 6A illustrates Concanavalin A – mannose binding assay performed on CBSI. In this experiment we obtained a K_D = 84 ± 17 μM, which compares favorably with both previous BSI results (96 ± 4μM)[33] and calorimetry (265-470μM).[30] We attribute the slightly higher error in K_D for ConA-mannose binding to elements other than instrumental noise, such as age of protein, sample handling, incubation time/temperature, and temperature of measurement. Given the literature range for K_D determinations and typically published results, the measurement is well within acceptable experimental error. While the calorimetry results reported elsewhere were obtained in free solution, the measurement required quite large volumes of sample at high concentration (1 mL of 100 μM to 1 mM carbohydrate and 2 mL of 10−100 μM lectin) increasing both cost and the potential for error due to aggregation.

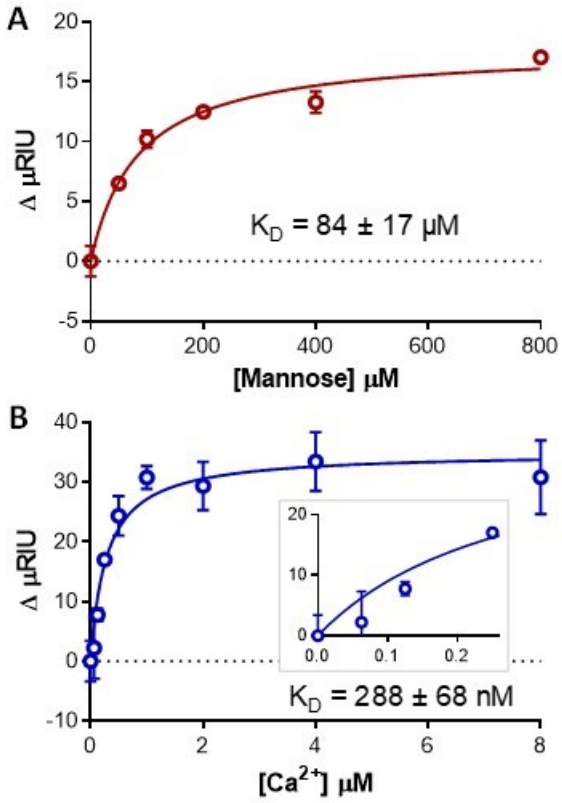

Figure 6. Binding assays performed on CBSI with no temperature control. A) Saturation isotherm of the Concanavalin A/Mannose interaction. B) Saturation isotherm of recoverin binding Ca^{2+}.

Next, we measured the well characterized ion - protein interaction, Ca^{2+} binding recoverin. This binding pair has previously been studied by both interferometric methods in free solution[34] and by the surface immobilized format SPR.[35]

Recoverin belongs to the family of NCS proteins and interacts with the N-terminal 25 amino acids of rhodopsin kinase (GRK1) thereby controlling phosphorylation of rhodopsin in a Ca^{2+}-dependent manner. It has been identified as an autoantigen in degenerative retinal diseases,[36] and previous studies of Recoverin in context of other neuronal calcium binding proteins have advanced the understanding of calcium-dependent conformational changes.[35]

The saturation isotherm measured for Ca^{2+}-recoverin interaction with CBSI is presented in Figure 6B. Here the K_D value was found to be 288 ± 68nM. This value is quite similar to previous determinations of apparent binding constant by fluorescence (270nM)[37] and 1.9μM by SPR.[35] SPR applications need immobilization of one interaction partner, which can create heterogeneous surfaces and might account for the larger variations observed with this technique. We have observed and quantified this phenomenon with BSI by comparing surface and free solution measurements of binding affinity.[33] However, CBSI enabled the quantification of Ca^{2+}-recoverin binding in free-solution providing affinity constants that are not impacted by any modification, such as immobilization or tagging with a fluorophore.

For further perspective on the two binding events presented, the highest concentration used for Mannose was 800 μM and the lowest concentration of Ca^{2+} ~60 nM. These concentrations span about 4 decades (from nearly a micromolar to 10s of nanomolar), illustrating the range of performance possible with CBSI operating in the absence of any temperature stabilization. Assuming 100% binding would mean that 60 nM of Ca-Recoverin had been formed and quantified. Thus, within the CBSI probe volume of 25nL there is merely 1.5 x 10^{-15} moles or 1.5 femtomoles of Ca-Recoverin detected by CBSI.

CONCLUSIONS

Here we demonstrated a compensated backscattering interferometer that is highly sensitive, has a nanoliter-volume, and enables mix-and-read biochemical assays in free solution and can be operated without temperature control, even in the presence to large environmental perturbations. The utility of the device was shown by characterizing the binding affinity of the ConA/Mannose and the Recoverin/Ca^{2+} systems. These affinity measurements provided results that compared favorably with previous affinity measurements, but with much less sample required, no need for surface immobilization, and no modification of either binding partner with a fluorophore. Two major advantages of CBSI are the simplicity of the optical train (laser, object and detector/camera) and the ability to function without temperature control. These properties are anticipated to facilitate miniaturization, resulting in a low cost, highly stable, field deployable system that is assay agnostic.

AUTHOR INFORMATION

Corresponding Author

* Email: darryl.j.bornhop@vanderbilt.edu

Author Contributions

All authors designed research. M.N.K., A.K.K. and I.R.O. performed research. M.N.K., D.J.B., and A.K.K. wrote the manuscript.

ACKNOWLEDGMENT

This work was supported under Grant no. 5R42GM090456-03 awarded by the National Institute of Health (NIH), under Grant no. CHE 1610964 awarded by the National Science Foundation (NSF).

REFERENCES

(1) Nitsche, C.; Otting, G. Nmr studies of ligand binding. *Curr Opin Struct Biol* **2017**, *48*, 16-22. DOI: 10.1016/j.sbi.2017.09.001.
(2) Ishii, K.; Noda, M.; Uchiyama, S. Mass spectrometric analysis of protein-ligand interactions. *Biophysics and physicobiology* **2016**, *13*, 87-95. DOI: 10.2142/biophysico.13.0_87.
(3) Cubrilovic, D.; Biela, A.; Sielaff, F.; Steinmetzer, T.; Klebe, G.; Zenobi, R. Quantifying protein-ligand binding constants using electrospray ionization mass spectrometry: A systematic binding affinity study of a series of hydrophobically modified trypsin inhibitors. *J Am Soc Mass Spectr* **2012**, *23*, 1768-1777. DOI: 10.1007/s13361-012-0451-6.
(4) Ababou, A.; Ladbury, J. E. Survey of the year 2005: Literature on applications of isothermal titration calorimetry. *Journal of molecular recognition : JMR* **2007**, *20*, 4-14. DOI: 10.1002/jmr.803.
(5) Di Trani, J. M.; Moitessier, N.; Mittermaier, A. K. Measuring rapid time-scale reaction kinetics using isothermal titration calorimetry. *Analytical chemistry* **2017**, *89*, 7022-7030. DOI: 10.1021/acs.analchem.7b00693.
(6) Wienken, C. J.; Baaske, P.; Rothbauer, U.; Braun, D.; Duhr, S. Protein-binding assays in biological liquids using microscale thermophoresis. *Nat Commun* **2010**, *1*, 10.1038/ncomms1093. DOI: 10.1038/Ncomms1093.
(7) Kussrow, A.; Enders, C. S.; Bornhop, D. J. Interferometric methods for label-free molecular interaction studies. *Analytical chemistry* **2012**, *84*, 779-792. DOI: 10.1021/ac202812h.
(8) Ciesielski, G. L.; Hytonen, V. P.; Kaguni, L. S. Biolayer interferometry: A novel method to elucidate protein-protein and protein-DNA interactions in the mitochondrial DNA replisome. *Methods in molecular biology* **2016**, *1351*, 223-231. DOI: 10.1007/978-1-4939-3040-1_17.
(9) Guerreiro, J. R. L.; Frederiksen, M.; Bochenkov, V. E.; De Freitas, V.; Sales, M. G. F.; Sutherland, D. S. Multifunctional biosensor based on localized surface plasmon resonance for monitoring small molecule-protein interaction. *ACS nano* **2014**, *8*, 7958-7967. DOI: 10.1021/nn501962y.
(10) Vashist, S. K.; Dixit, C. K.; MacCraith, B. D.; O'Kennedy, R. Effect of antibody immobilization strategies on the analytical performance of a surface plasmon resonance-based immunoassay. *The Analyst* **2011**, *136*, 4431-4436. DOI: 10.1039/C1an15325k.
(11) Bornhop, D. J.; Latham, J. C.; Kussrow, A.; Markov, D. A.; Jones, R. D.; Sorensen, H. S. Free-solution, label-free molecular interactions studied by back-scattering interferometry. *Science* **2007**, *317*, 1732-1736. DOI: 10.1126/science.1146559.
(12) Wang, M.; Kussrow, A. K.; Ocana, M. F.; Chabot, J. R.; Lepsy, C. S.; Bornhop, D. J.; O'Hara, D. M. Physiologically relevant binding affinity quantification of monoclonal antibody pf-00547659 to mucosal addressin cell adhesion molecule for in vitro in vivo correlation. *British journal of pharmacology* **2017**, *174*, 70-81. DOI: 10.1111/bph.13654.
(13) Bornhop, D. J.; Kammer, M. N.; Kussrow, A.; Flowers, R. A., 2nd; Meiler, J. Origin and prediction of free-solution interaction studies performed label-free. *Proc Natl Acad Sci USA* **2016**, *113*, E1595-1604. DOI: 10.1073/pnas.1515706113.
(14) Olmsted, I. R.; Hassanein, M.; Kussrow, A.; Hoeksema, M.; Li, M.; Massion, P. P.; Bornhop, D. J. Toward rapid, high-sensitivity, volume-constrained biomarker quantification and validation using backscattering interferometry. *Analytical chemistry* **2014**, *86*, 7566-7574. DOI: 10.1021/ac501355q.

(15) Estevez, M. C.; Alvarez, M.; Lechuga, L. M. Integrated optical devices for lab-on-a-chip biosensing applications. *Laser Photonics Rev* **2012**, *6*, 463-487. DOI: 10.1002/lpor.201100025.
(16) Lin, V. S.; Motesharei, K.; Dancil, K. P.; Sailor, M. J.; Ghadiri, M. R. A porous silicon-based optical interferometric biosensor. *Science* **1997**, *278*, 840-843. DOI: 10.1126/science.278.5339.840.
(17) Feng, J.; Siu, V. S.; Roelke, A.; Mehta, V.; Rhieu, S. Y.; Palmore, G. T. R.; Pacifici, D. Nanoscale plasmonic interferometers for multispectral, high-throughput biochemical sensing. *Nano Lett* **2012**, *12*, 602-609. DOI: 10.1021/nl203325s.
(18) Mariani, S.; Strambini, L. M.; Barillaro, G. Femtomole detection of proteins using a label-free nanostructured porous silicon interferometer for perspective ultrasensitive biosensing. *Analytical chemistry* **2016**, *88*, 8502-8509. DOI: 10.1021/acs.analchem.6b01228.
(19) Mariani, S.; Strambini, L. M.; Barillaro, G. Electrical double layer-induced ion surface accumulation for ultrasensitive refractive index sensing with nanostructured porous silicon interferometers. *ACS sensors* **2018**, *3*, 595-605. DOI: 10.1021/acssensors.7b00650.
(20) Li, D. F.; Feng, J.; Pacifici, D. Nanoscale optical interferometry with incoherent light. *Scientific reports* **2016**, *6*. DOI: 10.1038/Srep20836.
(21) Born, M.; Wolf, E. *Principles of optics: Electromagnetic theory of propagation, interference and diffraction of light*, 7th expanded ed.; Cambridge University Press: Cambridge ; New York, 1999, p xxxiii, 952 p.
(22) Guha, B.; Gondarenko, A.; Lipson, M. Minimizing temperature sensitivity of silicon mach-zehnder interferometers. *Optics express* **2010**, *18*, 1879-1887. DOI: 10.1364/OE.18.001879.
(23) Schneider, B. H.; Edwards, J. G.; Hartman, N. F. Hartman interferometer: Versatile integrated optic sensor for label-free, real-time quantification of nucleic acids, proteins, and pathogens. *Clin Chem* **1997**, *43*, 1757-1763.
(24) Baksh, M. M.; Kussrow, A. K.; Mileni, M.; Finn, M. G.; Bornhop, D. J. Label-free quantification of membrane-ligand interactions using backscattering interferometry. *Nature biotechnology* **2011**, *29*, 357-U173. DOI: 10.1038/Nbt.1790.
(25) Wang, Z.; Bornhop, D. J. Dual-capillary backscatter interferometry for high-sensitivity nanoliter-volume refractive index detection with density gradient compensation. *Analytical chemistry* **2005**, *77*, 7872-7877. DOI: 10.1021/ac050752h.
(26) Morcos, E. F.; Kussrow, A.; Enders, C.; Bornhop, D. Free-solution interaction assay of carbonic anhydrase to its inhibitors using back-scattering interferometry. *Electrophoresis* **2010**, *31*, 3691-3695. DOI: 10.1002/elps.201000389.
(27) Stjernstrom, M.; Roeraade, J. Method for fabrication of microfluidic systems in glass. *J Micromech Microeng* **1998**, *8*, 33-38. DOI: 10.1088/0960-1317/8/1/006.
(28) Markov, D.; Begari, D.; Bornhop, D. J. Breaking the $10^{(-7)}$ barrier for ri measurements in nanoliter volumes. *Analytical chemistry* **2002**, *74*, 5438-5441. DOI: 10.1021/ac020403c.
(29) Glière, A.; Delattre, C. Modeling and fabrication of capillary stop valves for planar microfluidic systems. *Sens Actuators, A* **2006**, *130-131*, 601-608. DOI: 10.1016/j.sna.2005.12.011.
(30) Schwarz, F. P.; Puri, K. D.; Bhat, R. G.; Surolia, A. Thermodynamics of monosaccharide binding to concanavalin a, pea (pisum sativum) lectin, and lentil (lens culinaris) lectin. *The Journal of biological chemistry* **1993**, *268*, 7668-7677.
(31) Sharon, N.; Lis, H. History of lectins: From hemagglutinins to biological recognition molecules. *Glycobiology* **2004**, *14*, 53R-62R. DOI: 10.1093/glycob/cwh122.
(32) Swanson, M. D.; Winter, H. C.; Goldstein, I. J.; Markovitz, D. M. A lectin isolated from bananas is a potent inhibitor of hiv replication. *The Journal of biological chemistry* **2010**, *285*, 8646-8655. DOI: 10.1074/jbc.M109.034926.
(33) Olmsted, I. R.; Kussrow, A.; Bornhop, D. J. Comparison of free-solution and surface-immobilized molecular interactions using a single platform. *Analytical chemistry* **2012**, *84*, 10817-10822. DOI: 10.1021/Ac302933h.
(34) Sulmann, S.; Kussrow, A.; Bornhop, D. J.; Koch, K. W. Label-free quantification of calcium-sensor targeting to photoreceptor guanylate cyclase and rhodopsin kinase by backscattering interferometry. *Scientific reports* **2017**, *7*, 45515. DOI: 10.1038/srep45515.
(35) Sulmann, S.; Dell'Orco, D.; Marino, V.; Behnen, P.; Koch, K. W. Conformational changes in calcium-sensor proteins under molecular crowding conditions. *Chemistry* **2014**, *20*, 6756-6762. DOI: 10.1002/chem.201402146.
(36) Polans, A. S.; Witkowska, D.; Haley, T. L.; Amundson, D.; Baizer, L.; Adamus, G. Recoverin, a photoreceptor-specific calcium-binding protein, is expressed by the tumor of a patient with cancer-associated retinopathy. *Proceedings of the National Academy of Sciences of the United States of America* **1995**, *92*, 9176-9180. DOI: 10.1073/pnas.92.20.9176.
(37) Permyakov, S. E.; Cherskaya, A. M.; Senin, II; Zargarov, A. A.; Shulga-Morskoy, S. V.; Alekseev, A. M.; Zinchenko, D. V.; Lipkin, V. M.; Philippov, P. P.; Uversky, V. N.; Permyakov, E. A. Effects of mutations in the calcium-binding sites of recoverin on its calcium affinity: Evidence for successive filling of the calcium binding sites. *Protein engineering* **2000**, *13*, 783-790. DOI: 10.1093/protein/13.11.783.

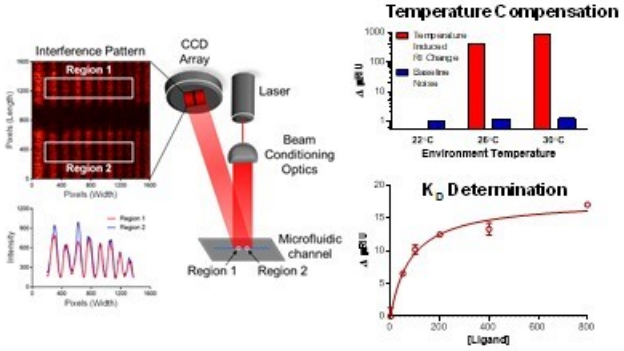

For TOC only